Int J Adv Manuf Technol (2017) 89:273–282
DOI 10.1007/s00170-016-9084-4

ORIGINAL ARTICLE

Comparative tests of the proper active grinding powers and maximum grinding temperatures, conducted on corrosion-resistant steel surfaces, using aluminium oxynitride and noble electrocorundum grinding wheels

Czesław Niżankowski[1] · **Grzegorz Struzikiewicz**[1]

Received: 10 May 2016 / Accepted: 16 June 2016 / Published online: 29 June 2016

Abstract This paper presents the results of comparative experimental tests of proper active powers and maximum temperatures, conducted on the circumference grinding of flat surfaces, made of grade 321 corrosion-resistant steel (1.4541), using modern aluminium oxynitride and noble electrocorundum vitrified-bonded grinding wheels. The tests were carried out in both up-cut and down-cut conditions. In both kinematic grinding aspects, the tested factors were determined by discrete increase of reductive grinding yield, applying increasing grinding-wheel in-feed to the workpiece and keeping the remaining grinding parameters at the constant level. The test results were later subjected to simplified statistical analysis, and an attempt was made at substantive test justification. It was demonstrated that, regardless of the assumed kinematic grinding aspects of steel grade 1.4541 (321), the values of all the comparatively tested values of aluminium oxynitride grinding wheels were, with increasing reductive grinding yield, lower than the corresponding values of the noble electrocorundum grinding wheels.

Keywords Electrocorundum grinding wheels · ALON grinding wheels · Active grinding power · Maximum grinding temperature · Stainless steel

✉ Grzegorz Struzikiewicz
struzikiewicz@mech.pk.edu.pl

Czesław Niżankowski
nizan@mech.pk.edu.pl

[1] Production Engineering Institute of the Mechanical Faculty, Cracow University of Technology, Al. Jana Pawła II 37, 31-866 Cracow, Poland

1 Introduction

White noble electrocorundum (α-Al_2O_3) was applied as grinding material on an industrial scale for the first time in France in 1902, while γ-aluminium oxynitride (γ-$Al_xO_yN_z$, in brief, ALON) was used for the first time in the USA in 1982 [1, 2].

Although the white noble electrocorundum production technology has not been subjected to considerable changes and it is still melted from technical alumina, with additives, in an electric arc furnace, aluminium oxynitride can be currently produced under about a dozen of various patented technologies allowing to obtain abrasives with diverse physical and chemical properties.

A detailed review of particular ALON abrasive production technologies, with the indication of property descriptions, is presented in the literature quoted by Nadolny [3].

Presently, the most popular in Europe and the Americas is the ALON abrasive traded under the name of ABRAL©, produced by the Pechiney Electrometallurgy Abrasives & Reflections and the Rio Tinto Alcan in France. ABRAL© is obtained with the application of direct aluminium nitriding, with small addition of titanium carbide, and sintering of fine crystallites in an electric furnace. The comparison of the basic properties of abrasive grains of ABRAL© 55N and of white noble electrocorundum 56A is presented in Table 1 [1–6] (Figs. 1 and 2).

The essential operating features which distinguish the aluminium oxynitride abrasives from those of noble electrocorundum include much lower wettability of the ALON grain surfaces by liquid chromium steel and lower intensity of grain microhardness loss zone, with increasing grinding temperature (Fig. 3).

Table 1 Comparison of the basic properties of abrasive grains of white noble electrocorundum 56A and of ABRAL 55N

Property	Noble electrocorundum 56A	Aluminium oxynitride ABRAL©
Grain shape	Sword-shaped[a]	Isometric[a]
Size of crystallites in grains (μm)	~10	~10
Grain density (g/cm^3)	3.96	3.65
Knoop microhardness (GPa)	20.3	18.0
Chemical composition	Al_2O_3 99 %	$Al_xO_yN_z$ 99.5 %
	SiO_2 0.01 %	SiO_2 0.06 %
	Fe_2O_3 0.02 %	Fe_2O_3 0.03 %
	Na_2O 0.16 %	Na_2O 0.11 %
	CaO + MgO 0.02 %	

[a] Classification of abrasive grain shapes according to [18]

Besides, aluminium oxynitride displays lower brittleness than does noble electrocorundum, and single grains show a larger number of cutting edges owing to sinter structure [3, 6].

The Austrian company Rappold-Winterthur applying both types of abrasives has been producing modern vitrified bonded grinding wheels for nearly 10 years.

Such grinding wheels made of noble electrocorundum are called Uwin, and those made of aluminium oxynitride are called NanoWin [1].

In comparison to the grinding wheels on classical ceramic binders, the grinding wheels in question are characterised by lower weight, higher resistance, ca. 10 % higher pore volume, higher resistance to tearing, and, consequently, the better machining ability at higher grinding speeds. Such grinding wheels make it also easier to supply cutting oil and coolant through the grinding wheel pores to the grinding zone.

Useful Uwin and NanoWin features result from the properties of the vitro crystalline binder bridges (Fig. 4) [7].

Such bridges are not only displaying higher degree adhesion to abrasive grains and lower volume in comparison to classical ceramic-binder grinding-wheel bridges, but they also contain vitro-crystalline phase fibre chains, distributed randomly in amorphous base. Those fibres positively affect the Uwin and NanoWin grinding wheel resistance to tearing and increase their durability. Besides, according to the research conducted in the Kraków University of Technology in Poland, the fibres hardly support micromachining processes [5–8].

The tests conducted by the Rappold-Winterthur Company, in respect of several different steel grades used in grinding processes, with the use of Uwin and NanoWin grinding wheels made of ABRAL© (ALON) and microcrystalline sintered alumina (Cubitron) abrasives, indicated that the grinding wheels made of aluminium oxynitride allowed to increase reductive grinding yield, decrease the machining time, and reduce the risk of grinding burns [1, 3, 7].

The reduction of the probability of grinding burn occurrence was associated with the reduction of grinding power according to the same test results.

However, as the Rappold-Winterthur Company did not publish the data concerning the testing conditions or detailed forms of the assumed evaluation indicators, the test results seem to be unclear and they require detailed verification.

Fig. 1 Dominating noble electrocorundum 56A abrasive grain shapes [1]

2 Research description

Figure 5 presents the testing diagram of the circumference surface grinding process, using the Uwin grinding wheel made of noble electrocorundum 56A and the NanoWin grinding wheels made of aluminium oxynitride 55N (ABRAL©). where

In the input value set X:

x_1—in-feed a_d (3, 5, 7, 9, 11, 13 μm)

In version I for an ALON grinding wheel, with the parameters 1A 250 × 33 × 76.2 55N 60 F15VPH 902W:

Ia—for up-cut grinding conditions

Fig. 2 Dominating abrasive grain shapes in aluminium oxynitride 55N—ABRAL© [1]

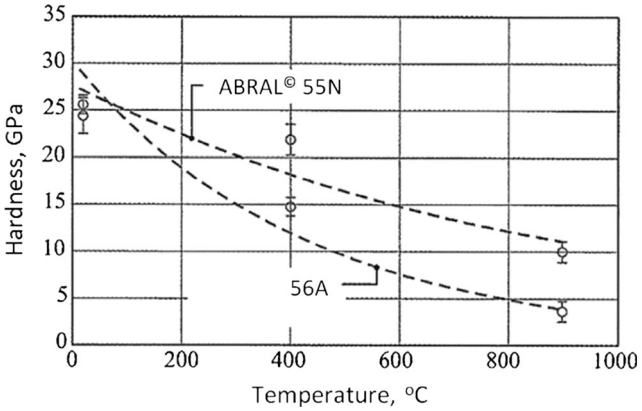

Fig. 3 Changes of grain microhardness in noble electrocorundum 56A and aluminium oxynitride 55N ABRAL©, depending on temperature [1, 3, 5]

Ib—for down-cut grinding conditions, version II for a 56A grinding wheel, with the parameters 1A 250 × 32 × 76.2 56A 60 F15VPH 902W:
IIa—for up-cut grinding conditions
IIb—for down-cut grinding conditions
In the input value set *Y*:
y_1—volumetric grinding yield Q_w mm^3
y_2—active grinding power Ps W
y_3—grinding temperature Θ in the maximum temperature zone

In the conversion input value set *Z*:

z_1—proper active grinding power $P_{sw} = \frac{P_s}{Q_w}\frac{W}{cm^3}$ [2, 7, 9]
z_2—average grinding temperature Θ_w in the maximum temperature zone
In the constant value set *C*:
c_1—grinder—precision grinder for surfaces, type 3G71S, Russian made
c_2—workpieces—100 × 20 × 20 mm cuboids made of corrosion-resistant steel 1H18N9T (1.4541, 321)
c_3—grinding velocity $v_s = 34$ m/s
c_4—longitudinal feed rate $f_t = 8$ m/min
c_5—cooling—without cutting oil and coolant
c_6—dressing parameters for active grinding wheel surfaces
c_7—dresser type—single-grain, diamond, ground with the blade weight of 0.8 karat
c_8—circumference surface grinding, without cross-feed (Fig. 6)

In the interfering value set *H*:

h_1—grinding wheel dispersion parameters
h_2—workpiece property value dispersion
h_3—grinding parameter setting dispersion
h_4—input value reading errors, etc.

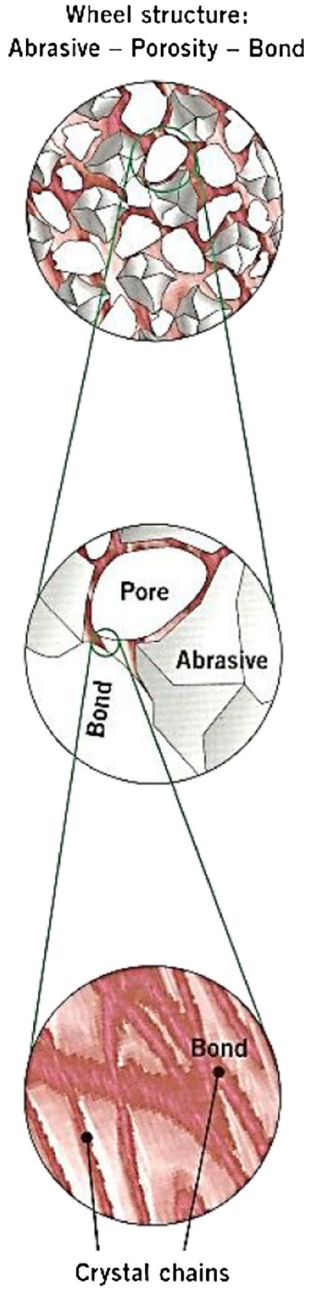

Fig. 4 The structure of Rappold-Winterthur vitro crystalline binders, series 600W and 900W [7]

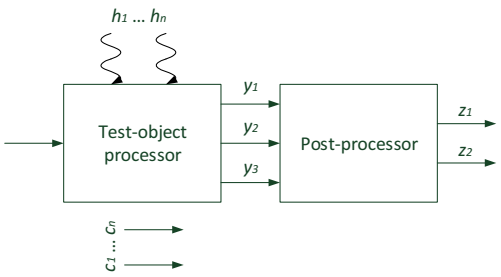

Fig. 5 Circumference surface grinding process testing diagram

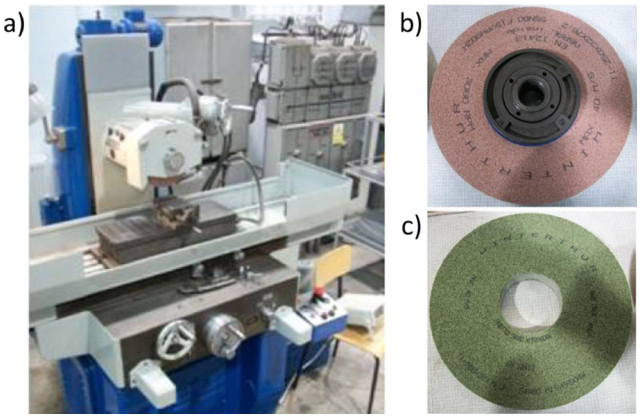

Fig. 6 Precision surface grinder, type 3G71S (**a**), 55N (**b**) and 56A grinding wheel (**c**)

2.1 Experimental test methodology

Experimental tests were conducted on all options and suboptions, in accordance with complete, static, determined Test Plan PS-DK [10]. In each Test Plan setting, each experiment was repeated three times. The test results obtained for each Test Plan option and suboption were subjected to approximation, with the use of the least square method and matrix calculus. Approximation was performed by the application of test object functions (TOF) in the form of the second-degree polynomials, without interaction, and exponential functions. The evaluation of the adequacy of the determined functions in respect of the measurement results was conducted on the basis of the analysis of maximum relative errors ε_{max} (Eq. 1) and determination coefficients R^2 (Eq. 2).

$$\varepsilon_{\max} = \max\left[\frac{\left|\left(\overline{z}^{u} - \check{z}^{u}\right)\right|}{\overline{z}^{u}}\right] \cdot 100\% \tag{1}$$

$$R^2 = \frac{\sum_{u=1}^{n}\left(\check{z}^{u} - \overline{z}\right)^2}{\sum_{u=1}^{n}\left(\overline{z}^{u} - \overline{z}\right)^2} \tag{2}$$

where

$\overline{z}^{u}$ is the arithmetic average of repeats in the Test Plan u-system

$\check{z}^{u}$ is the value calculated from the determined function in the Test Plan u-system

n is the number of Test Plan systems and $\overline{z}$ is based on Eq. (3):

$$\overline{z} = \frac{1}{n}\sum_{u=1}^{n}\overline{z}^{u} \tag{3}$$

The analyzed function was recognized to be adequate when the arbitrarily assumed allowed value of $\varepsilon_d \approx 20$ % was not lower than ε_{max}, and the value $R^2 \geq 0.95$.

2.2 Testing techniques

The volumetric grinding yield Q_w was determined arithmetically by multiplying the ground surface area by the grinding depth a_p. By using the coordinate machine measurement, it was found that $a_p \approx a_{d\text{-}0{,}0004}$ mm. The measurements of the active grinding power P_s were carried out by the application of a multi-functional wattmeter, type DW 6090 (Fig. 7), connected to the power-supply circuit of the main drive motor of the grinding wheel. The measurement results were read from the device's digital display. The grinding temperatures Θ were measured in the maximum temperature zone with the use of Flir S.C. 620 thermal imaging camera (Fig. 8), connected through a FireWire terminal to a microcomputer equipped with the ThermaCAM Researcher software. The software allowed to carry out a deep analysis of the determined temperature fields [11] (Fig. 9).

2.3 Test results

The first part of test results was presented analytically in Tables 2 and 3 for up-cut and down-cut grinding, respectively, with vitrified-bonded aluminium oxynitride grinding wheels.

Tables 4 and 5 present the second part of grinding test results for up-cut and down-cut grinding, respectively, with vitro-crystalline noble electrocorundum grinding wheels.

The test results presented here were subjected to approximation, in accordance with the previously discussed methodology and the approximating function courses, relative to in-feed (grinding depth), and they are illustrated in Figs. 10, 11, 12 and 13.

However, the values of proper active grinding powers are presented in Table 6 and Fig. 14, as the target test results for the grinding process with 55N grinding wheels and analogously, in Table 7 and Fig. 15, for the grinding process with 56A grinding wheels.

Next, according to the assumed evaluation methodology of the determined function adequacy, the values of maximum relative errors ε_{max} were calculated for the functions with the highest values of the determination coefficient R^2 and presented in Tables 8 and 9.

2.4 Substantive test result analysis

The definitely lowest values of active grinding powers and average temperatures in the maximum temperature zones, in the whole range of the applied grinding wheel in-feed towards the workpiece, during grinding with aluminium oxynitride grinding wheels, in comparison to the grinding processes with the use of noble electrocorundum grinding wheels (Figs. 10, 11, 12 and 13), resulted mainly from the differences in shape and material structures of the 55N (ALON-sintered microcrystallites) and 56A (composite poly-crystals) abrasive

Fig. 7 Multi-functional wattmeter DW 6090

grains. The ABRAL abrasive grains perform grinding with the base bundle in the form of "abrasive micro-needles", with very small edge radii and large friction resistance of the workpiece against the surface of such microstructures [1, 5, 8, 9, 12]. That means that micromachining phenomena dominate during the grinding process with ALON grinding wheels. That is demonstrated by the pictures of grinding trace structures in the ground surfaces (e.g. in Fig. 16a), the profile graphs of the grinding trace cross section (e.g. in Fig. 16b) and the isometric images of the ground surface (e.g. in Fig. 16c).

However, the noble electrocorundum abrasive grains perform grinding with several blades at most, with considerably larger edge radii and smaller friction resistance of the workpiece against the cutting zone of those blades [1, 5, 8, 9, 12]. Such conditions favour the development of side bulging in the form of burrs. That means that a considerable portion of the microgrinding work is not designed for the removal of the workpiece material, but rather for the material's side relocation. Thus, microgrinding with subsequent abrasive grains often occurs along the traces filled with burrs strengthened by the workpiece crush. Also in that case, this interpretation can be supported by the images of the grinding trace structures occurring on the ground surfaces (e.g. in Fig. 17a), the profile graphs of the grinding trace cross sections (e.g. in Fig. 17b) and the isometric images of the ground surface (e.g. in Fig. 17c).

Fig. 8 Flir SC620 thermal imaging camera

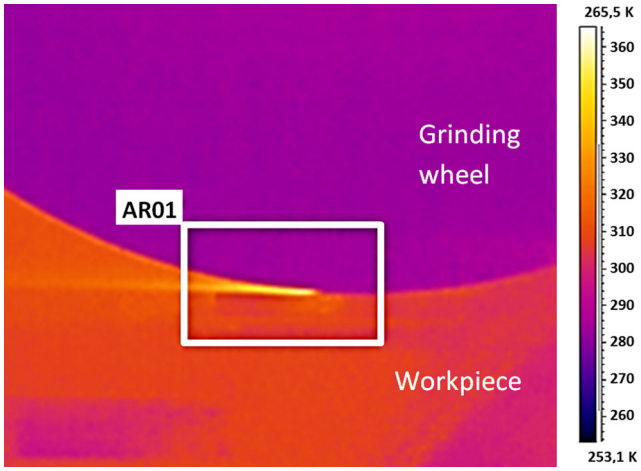

Fig. 9 Sample thermal image of the grinding zone

The above analysis explains not only the observed differences in active grinding powers but also the differences in the average temperature values in the maximum temperature zone. The sample temperature value differences occurring in particular temperature field zones, displayed in comparable grinding processes, are presented in the thermographs below (Figs. 18a, b).

However, considerably lower values of active grinding powers and average temperatures in the maximum temperature zone during down-cut and circumference grinding of flat steel surfaces, in comparison to up-cut grinding, regardless of the types of abrasives applied in the respective tests, resulted from the fact that abrasive grains start work with zero grinding

Table 2 Test results for up-cut grinding with ALON grinding wheels

a_d mm	Q_w mm^3	P_s W	Θ K
0.003	6	660	384
		708	354
		691	372
0.005	10	798	399
		893	381
		1080	344
0.007	14	1371	419
		1458	397
		1399	354
0.009	18	1845	434
		1656	419
		1738	404
0.011	22	2373	494
		2119	478
		1914	444
0.013	26	2283	519
		2055	500
		2123	464

Table 3 Test results for down-cut grinding with ALON grinding wheels

a_d mm	Q_w mm^3	P_s W	Θ K
0.003	6	627	376
		621	401
		603	409
0.005	10	582	365
		615	424
		609	419
0.007	14	906	411
		849	409
		874	437
0.009	18	1440	452
		1365	439
		1401	463
0.011	22	1419	496
		1388	489
		1137	459
0.013	26	1335	530
		1644	521
		1848	507

Table 5 Test results for down-cut grinding with 56A grinding wheels

a_d mm	Q_w mm^3	P_s W	Θ K
0.003	6	663	375
		689	425
		747	437
0.005	10	777	416
		805	443
		849	469
0.007	14	1242	511
		1101	493
		1190	498
0.009	18	1059	524
		1569	539
		1316	514
0.011	22	2277	555
		2034	600
		2136	503
0.013	26	2586	561
		1989	572
		2391	584

depth in up-cut grinding, unnecessarily grinding the workpiece and consuming additional energy portions.

A separate profound analysis is required in respect of the non-monotonous change phenomena in proper grounding powers with the increase of the grinding wheel in-feed to the workpiece, identified during the course of testing. Those phenomena also occur in application of both aluminium oxynitride (55N) grinding wheels and noble electrocorundum (56A) grinding wheels, although non-monotonicity of such

Table 4 Test results for up-cut grinding with 56A grinding wheels

a_d mm	Q_w mm^3	P_s W	Θ K
0.003	6	759	365
		807	394
		861	398
0.005	10	1212	406
		1256	413
		1308	419
0.007	14	1767	494
		1818	412
		1754	389
0.009	18	2409	506
		2244	482
		2318	466
0.011	22	2682	506
		2652	514
		2690	482
0.013	26	2649	525
		2682	543
		2703	502

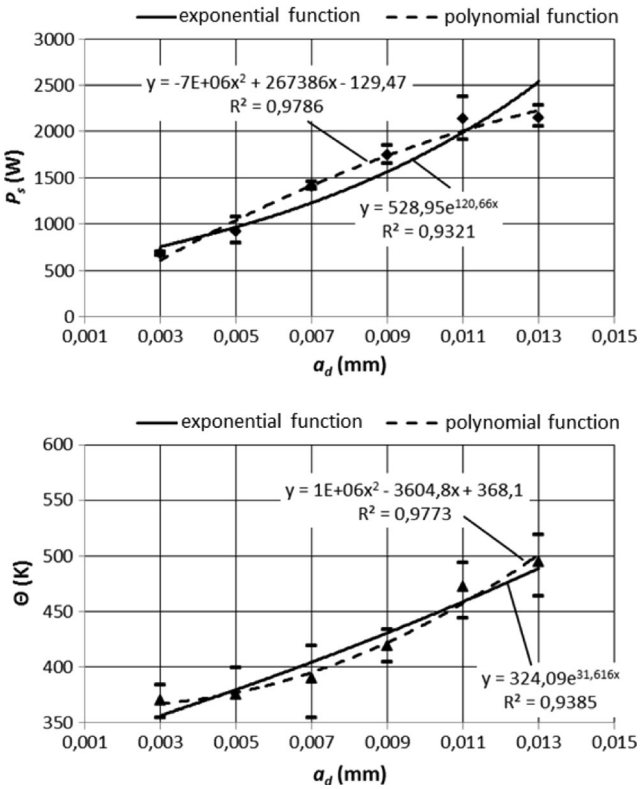

Fig. 10 The test-result approximating functions for up-cut grinding with 55N grinding wheels

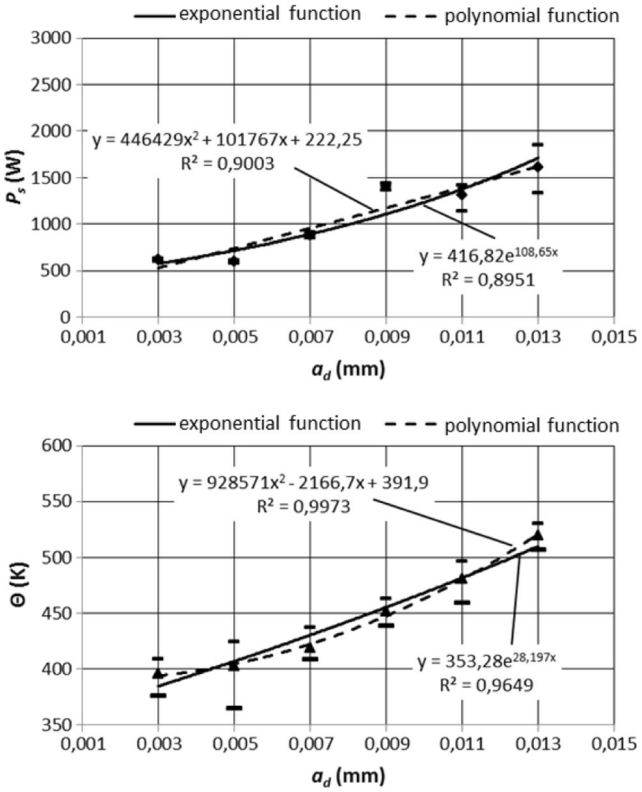

Fig. 11 The test-result approximating functions for down-cut grinding with 55N grinding wheels

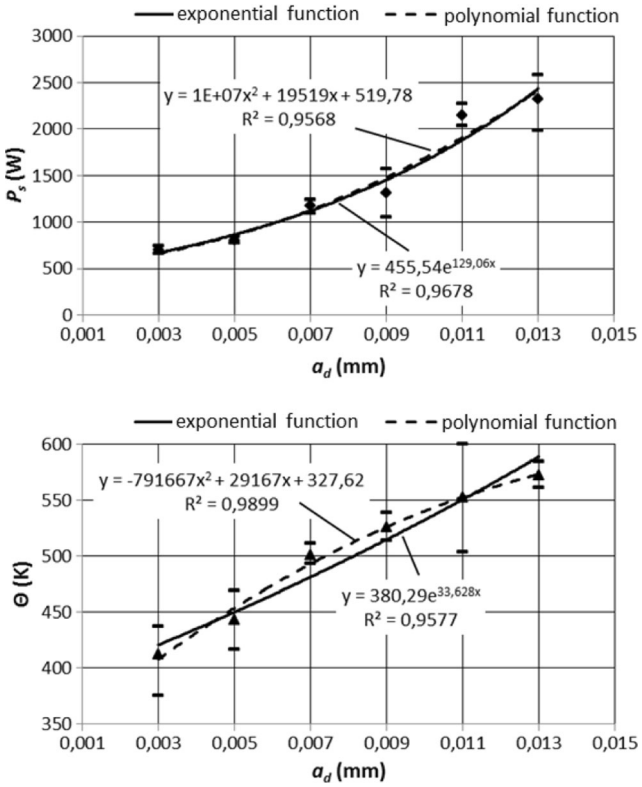

Fig. 13 The test-result approximating functions for down-cut grinding with 56A grinding wheels

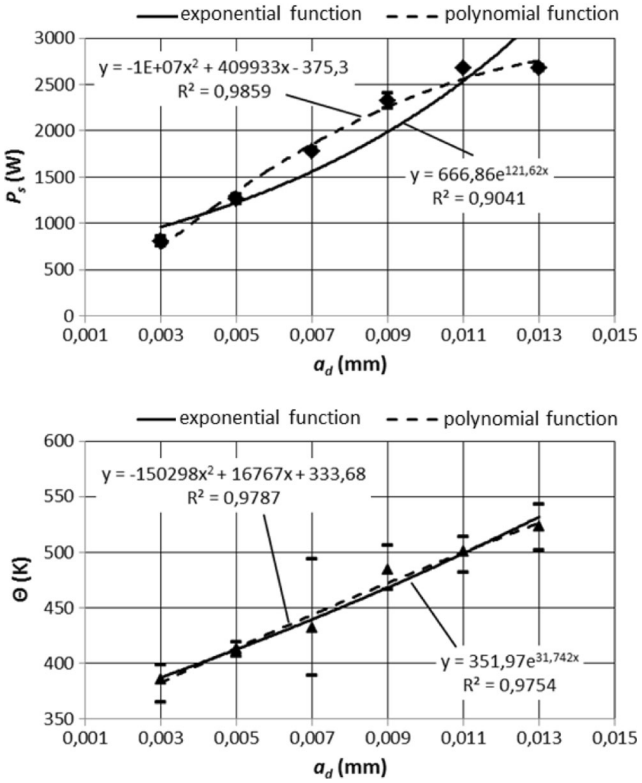

Fig. 12 The test-result approximating functions for up-cut grinding with 56A grinding wheels

Table 6 Proper active grinding power test results (55N grinding wheels)

a_d mm	P_{sw} w/mm^3	
	Up-cut	Down-cut
0.003	110.00	104.50
	118.00	103.50
	115.17	100.50
0.005	79.80	58.20
	89.30	67.50
	108.00	60.90
0.007	97.93	64.71
	104.14	60.64
	99.93	62.43
0.009	102.50	80.00
	92.00	75.83
	96.56	77.83
0.011	107.86	64.50
	96.32	63.09
	87.00	51.68
0.013	87.81	51.35
	79.04	63.23
	81.65	71.08

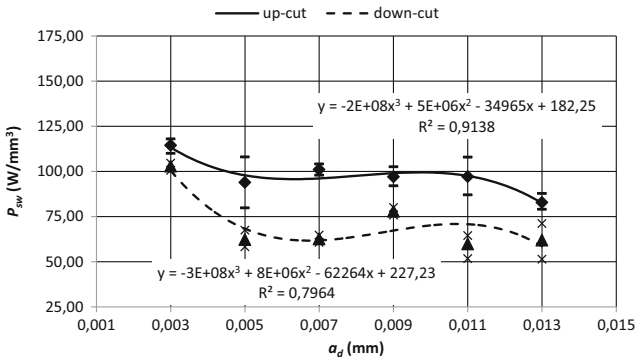

Fig. 14 Changes of the proper active power values in up-cut and down-cut grinding with 55N grinding wheels

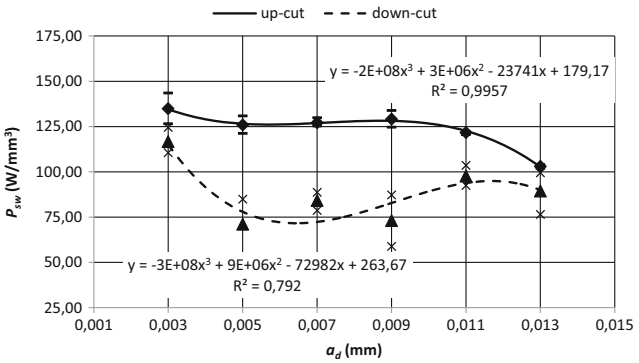

Fig. 15 Changes of the proper active power values in up-cut and down-cut grinding with 56A grinding wheels

changes is higher in down-cut grinding (Figs. 14 and 15). We can distinguish two minima in those non-monotonous changes. The first one corresponds to the in-feeds of the 5~7-μm range and the second one to the 13-μm in-feed. It would apparently seem that the non-monotonicity of changes in the proper grinding power results only from the form of functions approximating the test results (third-degree polynomials, without interaction). However, we should remember that the material which was used in the tests was corrosion-resistant steel grade 321, with austenitic structure, very low thermal conductivity and high microchip adhesion to the active grinding wheel surface (CPS).

The analysis of thermograms of the ground top surfaces and of the microchip shapes indicated the reasons of the occurrence of the first minima: it was the lowering of the proper microgrinding resistance, caused by a surge of the average temperature on the ground top surface, as a result of too slow thermal conductivity penetration into the workpiece (Fig. 19a, b).

However, the reason of the occurrence of the second minima was probably the attainment of the threshold of "support" of the microchip generation process due to intercrystalline corrosion, as well as the growth carbon solubility in the austenite (Figs. 18c) [13–17].

Table 7 Proper active grinding power test results (56A grinding wheels)

a_d mm	P_{sw} w/mm^3	
	Up-cut	Down-cut
0.003	126.50	110.50
	134.50	114.83
	143.50	124.50
0.005	121.20	77.70
	125.60	50.50
	130.80	84.90
0.007	126.21	88.70
	129.86	78.64
	125.29	85.00
0.009	133.83	58.83
	124.67	87.17
	128.78	73.11
0.011	121.91	103.50
	120.55	92.45
	122.27	97.09
0.013	101.88	99.46
	103.15	76.50
	103.96	91.96

3 Conclusions

The following conclusions were drawn from the present research:

- Together with in-feed (~grinding depth) increase, the values of active grinding power, volumetric grinding yield and temperature are increasing in the maximum temperature zone, regardless of the type of abrasive used in the tested grinding wheel or the kinematic grinding option under consideration. Such changes are correctly

Table 8 Maximum relative approximation errors for the relative active grinding power function

a_d mm	$\varepsilon_{max}(P_{sw})$			
	55 N		56A	
	Up-cut	Down-cut	Up-cut	Down-cut
0.003	13.9 %	15.2 %	11.2 %	10.5 %
0.005	4.4 %	20.7 %	8.9 %	2.2 %
0.007	4.0 %	5.6 %	10.2 %	7.7 %
0.009	7.3 %	18.5 %	3.9 %	4.1 %
0.011	17.2 %	1.6 %	8.7 %	14.6 %
0.013	5.2 %	12.3 %	20.7 %	4.7 %

Table 9 Maximum relative approximation errors for the maximum temperature function in the grinding zone

a_d mm	$\varepsilon_{max}(\Theta)$			
	55 N		56A	
	Up-cut	Down-cut	Up-cut	Down-cut
0.003	4.6 %	3.7 %	3.9 %	6.6 %
0.005	6.0 %	4.7 %	1.3 %	3.3 %
0.007	6.5 %	3.4 %	10.2 %	3.5 %
0.009	4.0 %	3.3 %	6.6 %	2.4 %
0.011	9.0 %	3.1 %	2.7 %	7.9 %
0.013	5.5 %	1.8 %	3.1 %	1.9 %

approximated by the test object functions, in the form of the second-degree polynomials; however, the active grinding power and temperature values in the maximum temperature zone are lower in the circumference grinding process, using the aluminium oxynitride grinding wheels,

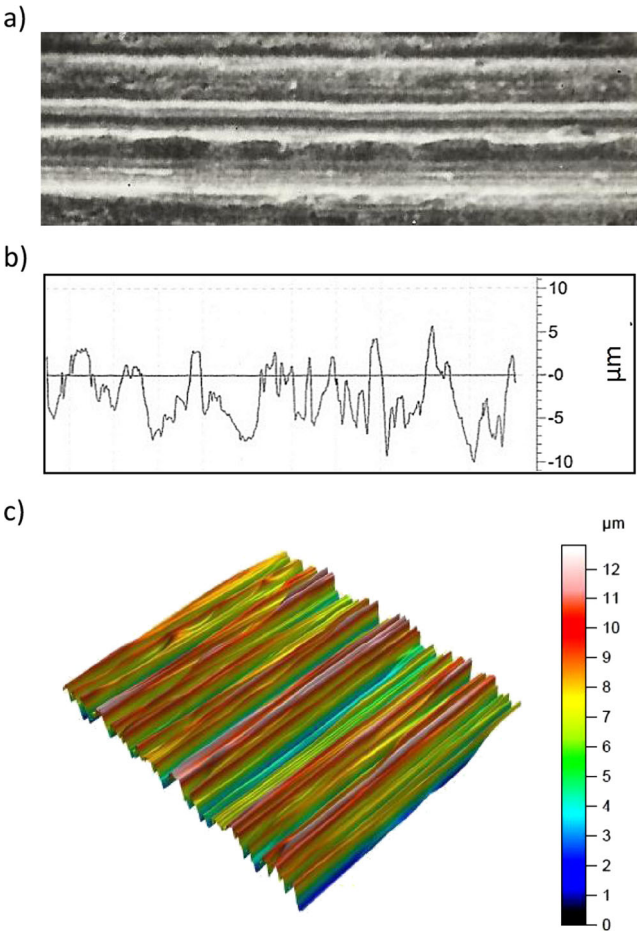

Fig. 16 The structure of grinding traces on the surfaces ground with aluminium oxynitride grinding wheels (**a**), profile graph of the grinding trace cross-section (**b**) and the isometric image of the ground surface (**c**)

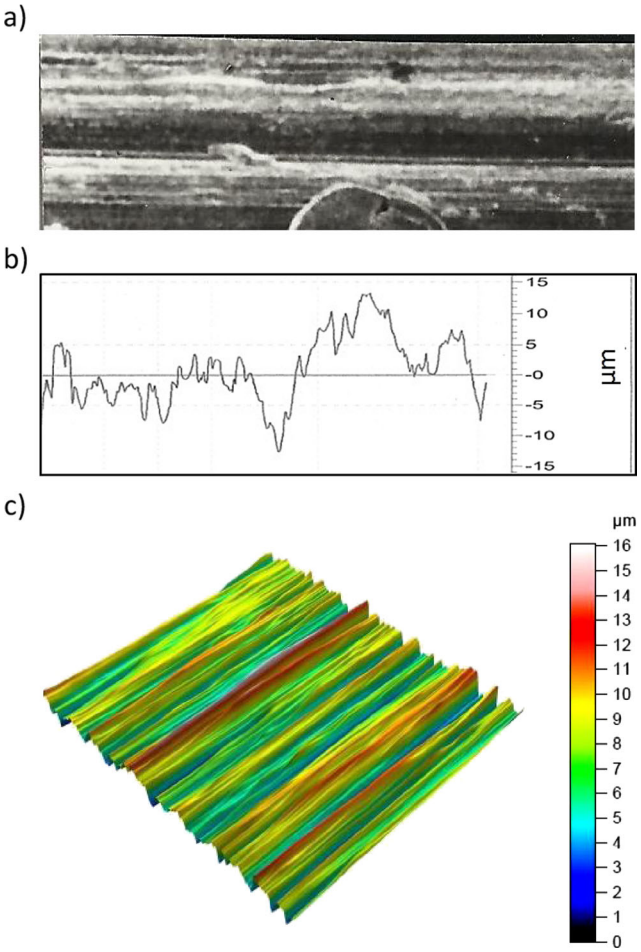

Fig. 17 The structure of grinding traces on the surfaces ground with noble electrocorundum grinding wheels (**a**), profile graph of the grinding trace cross-section (**b**) and the isometric image of the ground surface (**c**)

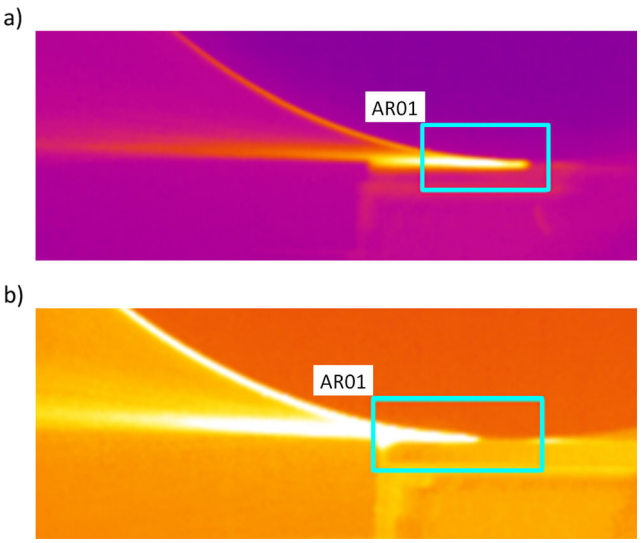

Fig. 18 Selected thermographs of the grinding zone, 55N (**a**) and 56A grinding wheels (**b**), for the grinding wheel in-feed to the workpiece of $a_d = 0.07$ mm

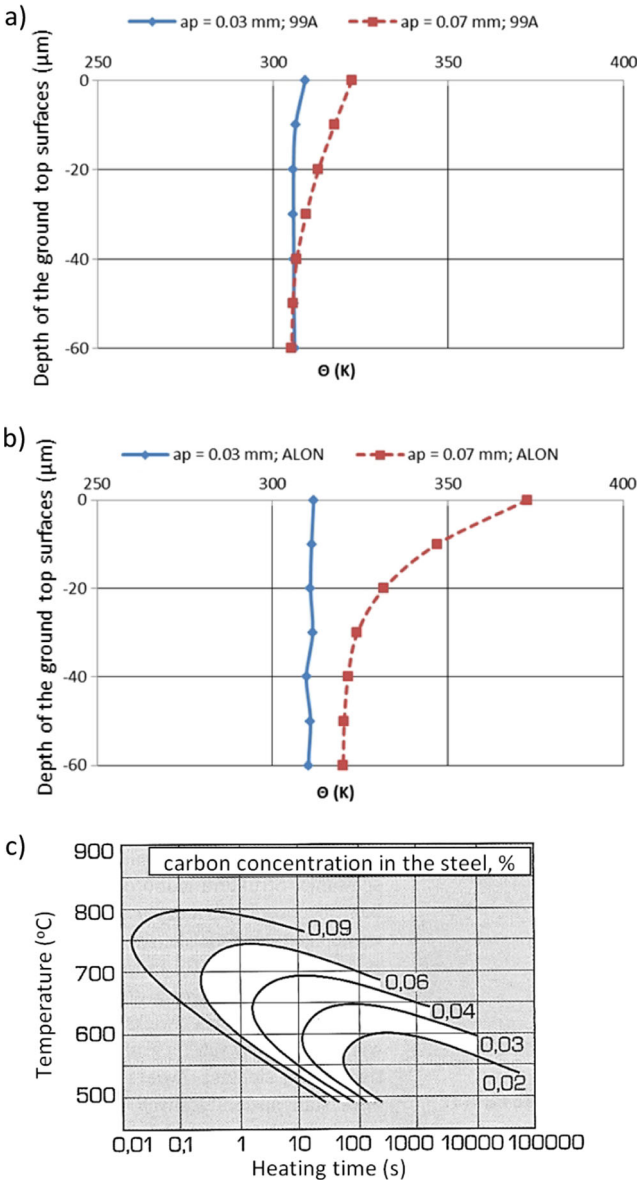

Fig. 19 Comparison of temperature gradients in the ground top surface during grinding with 3-µm (**a**) and 7-µm (**b**) feeds and the diagram TTS (time-temperature-sensitiveness on the corrosion) for 321 steel [14]

than in the analogous grinding process with the use of noble electrocorundum grinding wheels.

- Regardless of the types of abrasives applied in the tested vitro crystalline grinding wheels, the proper grinding power and average temperature values in the maximum temperature zone are lower during down-cut circumference grinding of steel grade 1H18N9T (321) flat surfaces than during the analogous up-cut grinding.
- Together with the in-feed (~ grinding depth) increase, the proper grinding power values are changing non-monotonously, regardless of the types of the abrasive used in the tested grinding wheel or the considered kinematic grinding option. Such changes are correctly approximated by the test object functions, in the form of the third-degree polynomials; however, the active grinding power values are lower in the circumference grinding process, using the aluminium oxynitride grinding wheels, than in the analogous grinding process with the use of noble electrocorundum grinding wheels.

References

1. Rappold-Winterthur Schulungsmaterialen (2013) Schleifscheibe von 55A und Schleifscheibe NanoWin®
2. Klocke F (2009) Manufacturing processes 2: grinding, honing, lapping. Springer Verlag, Berlin
3. Nadolny K (2012) Nowa generacja ziaren ściernych z azotkutlenku glinu, zwiększająca efektywność szlifowania, vol 8-9. Mechanik, Agencja Wydawnicza SIMP, Warszawa, pp 670–677
4. Roquefeuil F (2003) Abral. A new approach to precision grinding. Grinding and Abrasives Magazine. . Abrasives Magazine Inc, USA
5. Weinert K, Mohn T, Jansen T, Paffrath LU (2007) Abral-Schneidkorn steigert Effizienz beim Schleifen von Duplexstahl. Maschinenmarkt 113(11):28–31
6. Nadolny K, Sułowski P, Herman D (2012) Badania właściwości mechanicznych nowej generacji ziaren ściernych z azotku-tlenku glinu ALON z zastosowaniem sygnału emisji akustycznej, vol 8-9. Mechanik, Agencja Wydawnicza SIMP, Warszawa, pp 683–684
7. Graf W (2010) Handbook creep-feed and surface grinding. Wintherthur Technology Group Matteribach, Zurich
8. Webster J, Tricard M (2004) Innovations in abrasive products for precision grinding. Annals of the CIRP 53(2):597–617
9. Jackson MJ, Davim JP (2010) Machining with abrasives, 2014th edn. Springer, New York
10. Polański Z (1997) Planowanie Doświadczeń w Technice. PWN, Warszawa
11. Davies MA, Cao Q, Coke AI, Ivester R (2003) On the measurement and prediction of temperature fields in machining steel. Annals of the CIRP 52(1):77–80
12. Zorew NN, Kufarew GL, Goldschmidt MG (1967) Spannungszustand in der Schnitzone. Annals of the CIRP 14: 337–346
13. Nadolny K, Sułkowski P, Herman D (2015) Analysis of aluminium oxynitride ALON (Abral®) abrasive grains during the brittle fracture process using stress-wave emission techniques. Int J Adv Manuf Technol 81:1961–1976
14. Dobrzański L (2002) Podstawy nauki o materiałach i metaloznawstwo. Wydawnictwo Naukowo-Techniczne, Warszawa, p 637
15. Letner H (1995) Analysis of grinding quantities through chip sizes. J Mater Process Tech 95:1–7
16. Tso PL (1995) An investigation of chip types in grinding. J Mater Process Tech 53:521–532
17. Rowe WB (2009) Principles of modern grinding technology. William Andrew, Burlington
18. Woźniak K (1992) Materiały ścierne—wytwarzanie i własności. Wydawnictwo Naukowo-Techniczne, Warszawa, pp 97–239